Enhancing heat transfer in a high Hartmann number magnetohydrodynamic channel flow via torsional oscillation of a cylindrical obstacle

Wisam K. Hussam, Mark C. Thompson, and Gregory J. Sheard

Citation: Phys. Fluids **24**, 113601 (2012); doi: 10.1063/1.4767515
View online: http://dx.doi.org/10.1063/1.4767515
View Table of Contents: http://pof.aip.org/resource/1/PHFLE6/v24/i11
Published by the American Institute of Physics.

Enhancing heat transfer in a high Hartmann number magnetohydrodynamic channel flow via torsional oscillation of a cylindrical obstacle

Wisam K. Hussam,[1,2] Mark C. Thompson,[2] and Gregory J. Sheard[2,a)]
[1]*Department of Electromechanical Engineering, University of Technology, Baghdad, Iraq*
[2]*Department of Mechanical and Aerospace Engineering, Monash University, Victoria 3800, Australia*

(Received 3 June 2012; accepted 25 October 2012; published online 26 November 2012)

An approach is studied for side-wall heat transfer enhancement in the magnetohydrodynamic flow of fluid in a rectangular duct that is damped by a strong transverse magnetic field. The mechanism employs the rotational oscillation of a cylinder placed inside the duct to encourage vortex shedding, which promotes the mixing of fluid near a hot duct wall with cooler fluid in the interior. The effectiveness of the heat transfer enhancement is investigated over a wide range of oscillation amplitudes and forcing frequencies. The motivation for exploring this mechanism is inspired by the transient growth response of this flow, which indicates that the optimal disturbances feeding the vortex shedding process are localized near the cylinder, and are characterized by an asymmetrical disturbance with respect to the wake centreline. The results show that a considerable increase in heat transfer from the heated channel wall due to rotational oscillation of the cylinder can be achieved, with the maximum enhancement of more than 30% over a zone extending $10d$ downstream of the cylinder. As the angular velocity amplitude of oscillation is increased, the range of oscillation frequencies for effective enhancement is widened, and the frequency at which the peak Nusselt number occurs is shifted slightly to lower frequencies. As the amplitude is increased, the formation of strong discrete wake vortices draws fluid from the wall boundary layers into the wake, enhancing heat transfer. The effect of oscillation amplitude on the distribution of local Nusselt number Nu_w along the heated wall is significant. With an increase in Reynolds number, scope for additional heat transfer enhancement is possible. © *2012 American Institute of Physics*. [http://dx.doi.org/10.1063/1.4767515]

I. INTRODUCTION

Magnetohydrodynamic (MHD) flow through ducts in the presence of a transverse magnetic field has become important due to its engineering applications such as magnetohydrodynamic generators, pumps, metallurgical processing, and cooling of fusion reactors. Considering fusion reactors as an example, liquid metal may be used as a coolant and as a breeder material.[1] It circulates within the blanket and is exposed to the strong magnetic field used to confine the plasma. Under these conditions, the motion of the electrically conducting fluid induces electric currents, which interact with the applied magnetic field and produce electromagnetic forces that exert a retarding force on the flow. Therefore, magnetohydrodynamic duct flows can be characterized by laminar flow structures because velocity fluctuations are suppressed. However, the strong anisotropic feature of the electromagnetic forces leads to the formation of extended vortex tubes oriented parallel to the magnetic field.[2,3] These vortices are suppressed only weakly and can form quasi-two-dimensional structures in the plane perpendicular to the magnetic field. In addition to liquid-metal cooling systems

a)Greg.Sheard@monash.edu.

in fusion reactors, other liquid-metal duct flow applications include the cooling of nuclear fission reactors and high-performance computing infrastructure. Beyond MHD applications, channel flows exhibiting quasi-two-dimensional characteristics appear in applications ranging from microfluidics through to geophysical flows.

An avenue for exploiting quasi-two-dimensional flow structures to enhance heat transfer is to employ turbulence promoters, such as a bluff body placed inside the duct. The disturbances resulting from these promoters could increase the fluid mixing and disrupt the development of the thermal boundary layer resulting in an enhancement in heat transfer. This approach has been investigated experimentally[4–7] and numerically.[8,9] For the case with an insulated duct wall, Refs. 10 and 11 demonstrated that the heat transfer rate under a strong axial magnetic field was improved by more than twice that of the laminar flow. The heat transfer enhancement from the heated wall may be further increased if the vortex shedding in the flow is excited by perturbing the body placed within the flow. Consideration will now be given to cylinder oscillation as a perturbation mechanism.

For the case without a magnetic field, a limited number of studies have investigated the vortex dynamics of an oscillating cylinder in a straight channel, and the studies relevant to heat transfer enhancement in a straight channel using an oscillating obstacle are very rare. To the best of the authors' knowledge, there is no study on the flow and heat transfer characteristics of MHD flow past an oscillating cylinder in a channel. In the absence of both cylinder rotation and a magnetic field, the hydrodynamic flow at the Reynolds numbers of interest in this study is highly time-dependent, with strong vortex shedding behind the cylinder invoking strong mixing and heat transfer due to velocity fluctuations interacting with the heated side-wall boundary layer. The damping effect of the magnetic field decreases heat transfer and convection velocities.[9,12,13]

Yang[14] investigated numerically the heat transfer enhancement in a channel under the effect of a transversely oscillating square cylinder for a constant blockage ratio $\beta = 0.25$ and constant Prandtl number $Pr = 0.71$ for Reynolds numbers varying from 100 to 800. The oscillation frequency, oscillation amplitude, and maximum speed of the bar were examined to analyze the flow structures and the heat transfer enhancement. A remarkable heat transfer enhancement with increasing oscillation amplitude was reported with overall heat transfer increment of 57%. This was due to the formation of transverse vortices downstream of the bar, which transported the low-temperature and high-speed flow in the center of the duct toward the heated region of the channel. Consequently, the high-temperature fluid was convected away from the heated regions of the channel to mix with the low temperature core flow.

Using a moving boundary formulation and the arbitrary Lagrangian method modified by Yang,[14] Fu and Tong[15] performed a numerical simulation to study the effect of the flow passing a transversely oscillating circular cylinder on the heat transfer enhancement in a horizontal heated blocked channel for a blockage ratio $\beta = 0.25$, and the Reynolds number was varied between 100 and 500. Their results indicated that the heat transfer rate was improved substantially in the lock-in regime with heat transfer increments in some cases of more than 100%. They also found that the influence of the oscillation amplitude of the cylinder on the heat transfer rate was remarkable when the amplitude was larger than 0.1.

More recently, the heat transfer enhancement in a heated slot channel due to vortices shed from a transversely oscillating circular cylinder was investigated[16] for a constant blockage ratio $\beta = 0.3$ at Reynolds number $Re = 100$ in the Prandtl number range $0.1 \leq Pr \leq 10$. The cylinder oscillation amplitude was kept constant, while the frequency of the oscillation was varied from 0.75 to 1.25 relative to the Strouhal frequency of a fixed circular cylinder. Their results demonstrated that the transverse oscillations of a cylinder significantly enhanced heat transfer, and the maximum augmentation was observed to occur at the frequency $f_e = 0.75$. They ascribed this to the presence of high-intensity vortices near the channel walls, which have a significant effect on the heat transfer enhancement from the walls.

In this study, the fundamental behavior of a mechanism for heat transfer enhancement in damped quasi-two-dimensional steady-state duct flows will be examined. The perturbation method employs the rotational oscillation of a cylinder placed in the duct, and the resulting dynamics and heat transfer enhancement are investigated over a wide range of oscillation amplitudes and forcing frequencies. The motivation for exploring this mechanism was inspired by a recent transient growth analysis,[17]

which demonstrated that the optimal disturbances leading to the production of vortex shedding are localized near the cylinder, and are characterized by an asymmetrical disturbance with respect to the wake centreline.

II. PROBLEM DEFINITION

The configuration of the physical system to be considered is shown in Fig. 1. A circular cylinder of diameter d is placed on the centreline of a duct parallel to the magnetic field and perpendicular to the flow direction. A torsional oscillation is imposed on the cylinder about its own axis. The out-of-plane channel depth is a, and the duct cross-section is taken to have a height to depth ratio $h/a = 2$ throughout this study. The duct walls and the cylinder are assumed to be electrically insulated. A uniform homogeneous axial magnetic field with a strength B is imposed along the cylinder axis. One of the walls oriented parallel to the magnetic field is heated to a constant wall temperature T_w whereas the other surfaces are kept at a constant temperature T_0. The magnetic Reynolds number Re_m (which represents the ratio between the induced and the applied magnetic field) is assumed to be very small. Hence, the induced magnetic field is negligible and spatial variation in the magnetic field can be neglected.[18] Under these conditions, the flow is quasi-two-dimensional and consists of a core region, where the velocity is invariant along the direction of the magnetic field, and thin high-shear Hartmann layers are located at the walls perpendicular to the magnetic field. The quasi two-dimensional model[2] is constructed by averaging the flow quantities along the magnetic field direction.

Under this model, the non-dimensional magnetohydrodynamic equations of continuity, momentum, and energy reduce to

$$\nabla \cdot \mathbf{u} = 0, \tag{1}$$

$$\frac{\partial \mathbf{u}}{\partial t} + (\mathbf{u} \cdot \nabla)\mathbf{u} = -\nabla p + \frac{1}{Re}\nabla^2 \mathbf{u} - 2\frac{Ha^\star}{Re}\mathbf{u}, \tag{2}$$

$$\frac{\partial T}{\partial t} + (\mathbf{u} \cdot \nabla)T = \frac{1}{Pe}\nabla^2 T, \tag{3}$$

where $\mathbf{u}$, p, and T are the velocity, kinematic pressure, and temperature fields, respectively, projected onto the x-y plane. The modified Hartmann number is defined as

$$Ha^\star = \left(\frac{d}{a}\right)^2 Ha. \tag{4}$$

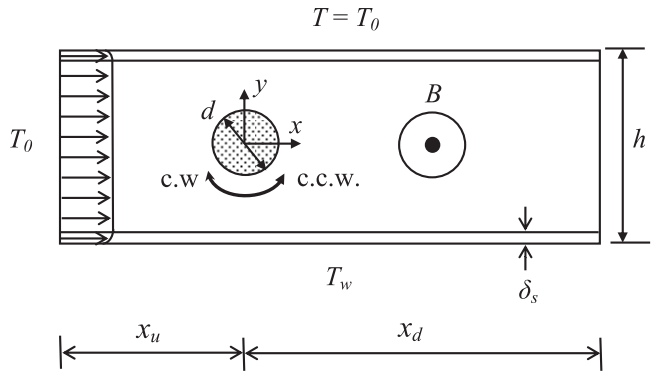

FIG. 1. The physical model of the torsionally oscillating cylinder. The magnetic field B acts in the out-of-plane direction, parallel to the cylinder axis. δ_S is the thickness of the Shercliff layer, and h and d are the duct width and cylinder diameters, respectively. Throughout this study, the blockage ratio $\beta = d/h = 0.303$. The upstream and downstream lengths are $x_u = 8d$ and $x_d = 25d$, respectively.

Here, lengths are scaled by the cylinder diameter d, pressure by ρU_0^2, where ρ is the density and U_0 is the peak inlet velocity, time by d/U_0, and temperature by the imposed temperature difference between the bottom and top walls, ΔT.[13,19] It is noted that the energy equation is sometimes written to include terms describing the effects of viscous dissipation and Joule heating (e.g., see Hossain[20]). However, these terms are not considered in this study (following Refs. 13, 21, and others), as their contributions are negligible for the application considered in this study.[11] Having imposed no constraint on the orientation of the channel, and following Refs. 13, 22, and 23, the influence of natural convection is not considered in the present study. Reference 12 provides further guidance with respect to the effect of natural convection. They demonstrate that for MHD flow in a vertically aligned duct, at Hartmann numbers $Ha \gtrsim 400$ (such as those considered in this study), natural convection is negligible for Rayleigh numbers less than $Ra \approx 10^4$. For $Ra \gtrsim 10^4$, the Nusselt number associated with natural convection remained consistently less than that for an equivalent channel without a magnetic field.

The dimensionless parameters, Reynolds number, Hartmann number, and Péclet number, are, respectively, defined as

$$Re = \frac{U_0\, d}{\nu}, \tag{5}$$

$$Ha = a\, B \sqrt{\frac{\sigma}{\rho \nu}}, \tag{6}$$

$$Pe = Re\, Pr, \tag{7}$$

where ν, σ, B, and a are the kinematic viscosity, magnetic permeability of the liquid metal, applied magnetic field, and half the out-of-plane duct height, respectively. The Prandtl number $Pr = \nu/\kappa_T$, where κ_T is the thermal diffusivity of the fluid.

The local Nusselt number along the lower heated wall of the channel is defined as

$$Nu_w(x, t) = \frac{d}{(T_f - T_w)} \left.\frac{\partial T}{\partial y}\right|_{wall}. \tag{8}$$

T_f is the bulk fluid temperature, which is calculated using the velocity and temperature distribution as

$$T_f(x, t) = \frac{\int_0^h uT \,\mathrm{d}y}{\int_0^h u \,\mathrm{d}y}, \tag{9}$$

where h is the width of the duct, and u is the streamwise component of velocity.

A time-averaged Nusselt number for heat transfer through the heated wall of the channel is calculated by first taking the time average of the local Nusselt number ($\overline{Nu}_w$) at each x-station, and then integrating over the length of the heated bottom wall, L, using

$$Nu = \frac{1}{L} \int_0^L \overline{Nu}_w(x) \,\mathrm{d}x. \tag{10}$$

To characterize the effect on the heat transfer due to the addition of a cylinder to the channel, the overall increment of heat transfer is defined as

$$HI = \frac{Nu - Nu_s}{Nu_s} \times 100, \tag{11}$$

where Nu_s is a reference time-averaged Nusselt number (e.g., the heated region of the same duct without cylinder rotation, i.e., $A = 0$).

The lift and moment coefficients are calculated from

$$C_L = \frac{F_l'}{\frac{1}{2}\, \rho u_0^2 d}, \tag{12}$$

$$C_M = \frac{M'}{\frac{1}{4}\, \rho u_0^2 d^2}, \tag{13}$$

where F_l' and M' are the lift and moment exerted by the fluid per unit length of the cylinder. The total force acting on the cylinder surface is due to pressure and viscous component, which can be computed by direct integration over the surface of the cylinder.[24,25] This leads to the moment contribution

$$\mathbf{M} = \oint \mathbf{r} \times (p\,\mathbf{n} + \tau_w)\,\mathrm{d}s, \tag{14}$$

where $\mathbf{n}$ is the unit outward vector normal of the fluid domain, $\mathbf{r}$ is a moment arm vector, p is the pressure field, τ_w is the wall friction, and ds represents a surface increment around the cylinder.

Since the cylinder is rotated sinusoidally in time at a forcing frequency f_e, the angular velocity of the cylinder is expressed as

$$\dot{\boldsymbol{\theta}}_{\mathrm{cyl}} = A\sin(2\pi f_e t), \tag{15}$$

where A and $\dot{\boldsymbol{\theta}}$ are non-dimensionlized by U_0/d. The maximum tangential surface speed of the cylinder is therefore given by $A(U_0/d)(d/2) = A(U_0/2)$, and the angular amplitude of displacement of the oscillation is given by $A(U_0/d)/(2\pi f_e) = A/(2\pi St_e)$, where the Strouhal number characterizing oscillation frequencies is given by

$$St_e = \frac{f_e d}{U_0}. \tag{16}$$

The fluid structure and heat transfer characteristics are investigated for quasi two-dimensional channel flow for a reference case taken to have $Re = 1075$, $Ha^\star = 151.5$, and $\beta = 0.303$. The angular velocity amplitude is varied over the range $0 \le A \le 3$, while the forcing frequency is varied over $0 \le St_e \le 10$. However, to focus on important results, vorticity and temperature contours are presented only for cases where the maximum heat transfer occurred. A Prandtl number $Pr = 0.022$ is used throughout, representative of the eutectic alloy GaInSn.

III. NUMERICAL METHODOLOGY

A nodal spectral-element method is utilized to discretize the governing flow and energy equations in space, and a third-order scheme based on backwards differentiation is employed for time integration.[26]

The boundary conditions imposed on Eqs. (1)–(3) are as follows: a no-slip boundary condition for velocity is imposed on all solid walls. At the channel inlet, the analytical solution to Eqs. (1) and (2) for fully-developed flow in a channel without a cylinder is imposed, following Ref. 9. At the exit, a constant reference pressure is imposed and a zero streamwise gradient of velocity is weakly imposed through the Galerkin treatment of the diffusion term of the momentum equation. A high-order Neumann condition for the pressure gradient is imposed on the Dirichlet velocity boundaries to preserve the third-order time accuracy of the scheme.[26] On the cylinder wall, a periodic torsional oscillation is imposed. The temperature of the incoming stream and top wall is taken as T_o, and at the bottom wall as T_w. The cylinder is thermally insulated (i.e., a zero normal temperature gradient is imposed at its surface).

The computational domain is divided into a grid of elements. Elements are concentrated in areas of the domain that experience high velocity gradients. The mesh representing the elemental discretization of the computational domain is shown in Fig. 2.

A convergence study for spatial resolution has been performed by varying the element polynomial degree from 4 to 9, while keeping the macro element distribution unchanged. The maximum lift coefficient $C_{L,\,\max}$, maximum moment coefficient $C_{M,\,\max}$, and the time-averaged Nussult number along the heated wall Nu were monitored. Convergence tests were performed for an oscillation amplitude $A = 3$, $St_e = 0.2$, $Re = 1075$, $Ha^\star = 151.5$, and $\beta = 0.303$. The results are presented in Table I. It is found that the results are converged to within less than 0.5% with polynomial order $N_p = 7$, which is hereafter used for the simulations reported in this study.

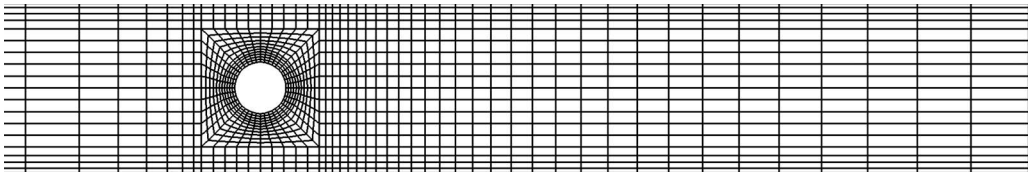

FIG. 2. Spectral element mesh of the computational domain. The mesh extends $8d$ upstream and $25d$ downstream of the cylinder. Within each element shown here, a grid of interpolation points resolves the high-order tenseor product of polynomial shape functions used to describe the flow fields.

A. Validation of the numerical system

The numerical system has been validated for the flow and heat transfer of stationary cylinder in both an open flow and confined within a channel for cases with and without a magnetic field. The details of these may be found in Refs. 11, 27, and 28. In addition to these, the heat transfer generated by a rotating oscillating cylinder in an open, non-MHD flow was tested. Computed average Nusselt numbers Nu for heat transfer with $Pr = 0.7$ for $A = 0.78$ and 1.57 at $Re = 100$ and 200 were compared against an earlier numerical study.[29] The mean percentage differences between the Nu predicted by the present simulations and those of the previous study was less than 1%. These studies demonstrate the reliability of the present solver.

IV. RESULTS AND DISCUSSION

A. Effects of oscillation frequency and amplitude on heat transfer

To begin, Nusselt numbers are computed for a wide range of velocity amplitudes A and forcing frequencies St_e. The velocity amplitude is varied over the range $0 \leq A \leq 3$, while the forcing frequency is varied over $0 \leq St_e \leq 10$. These ranges of parameters are consistent with the ranges employed in previous studies in which the torsional oscillation of a cylinder in a free stream flow[29] has been considered.

The time-averaged Nusselt number for a broad range of forcing frequency St_e is shown in Fig. 3 for a selection of oscillation amplitudes. Note that without cylinder rotation, the flow remains steady for the combination of parameters employed in this study. Incidentally, this corresponds to $St_e = 0$ in this plot. For reference, the critical Reynolds number for the onset of vortex shedding at this β and Ha is $Re_c = 1100$. The figure shows that there is a significant enhancement in heat transfer obtained for high amplitudes. Indeed a progressive increase in the peak Nusselt number is generated with increasing A. It is also interesting to observe that as the oscillation amplitude increases, the frequency producing peak heat transfer decreases, and a wider range of frequencies produces a noticeable heat transfer enhancement. For comparison, frequencies associated with both the dominant linear instability (St_{LSA}) and the optimal disturbance (St_{TG}) are each included in the plot. It can be seen that increasing A shifts the frequency for peak heat transfer enhancement away

TABLE I. Peak lift coefficient amplitude $C_{L,\max}$ and average Nusselt number along the heated wall Nu with varying polynomial order for a torsional oscillating cylinder at $Ha^{\star} = 151.5$, $Re = 1075$, $A = 3$, $St_e = 0.2$, and $\beta = 0.303$.

N_p	$C_{L,\max}$	$C_{M,\max}$	Nu
4	4.7330	0.6693	2.5451
5	4.6408	0.6788	2.5494
6	4.6608	0.6732	2.5553
7	**4.6766**	**0.6736**	**2.5617**
8	4.6768	0.6738	2.5616
9	4.6768	0.6740	2.5615

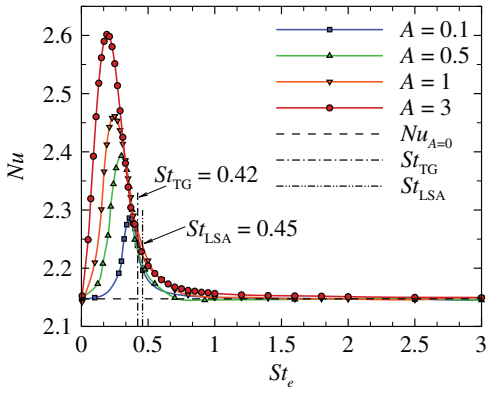

FIG. 3. Time-averaged Nusselt number plotted against cylinder oscillation frequency for different oscillation amplitudes for $Re = 1075$ and $Ha^\star = 151.5$. For reference, Nusselt number for the case of steady flow without oscillation ($St_e = 0$) is shown by the horizontal dashed line. Vertical lines denote frequencies obtained from evolving linearized perturbations from analysis of the fixed-cylinder case, where St_{TG} and St_{LSA} are seeded by the optimal perturbation from a transient growth analysis and the leading mode from a linear stability analysis, respectively.

from these frequencies, presumably as a result of non-linearity of the imposed disturbance to the flow imparted by the cylinder.

In Fig. 4(a), the peak heat transfer coefficient at each angular velocity amplitude, $Nu_{\max}$, is plotted against A. It can be observed that $Nu_{\max}$ increases significantly as A increases. This may be attributed to the fact that stronger vortices are generated behind the cylinder when it oscillates with larger amplitude, thanks to the higher shear between the moving cylinder surface and the flow during the part of the cycle where the cylinder moves against the flow. It is noted that the most rapid increases are formed for smaller A. Hence, there is a diminishing benefit in terms of further heat transfer enhancement as the amplitude is progressively increased.

The percentage increments to the overall heat transfer are approximately 6.5%, 11.5%, 15%, and 22% for $A = 0.1$, 0.5, 1.0, and 3.0, respectively, over that obtained for steady flow. The effect of increasing the amplitude on heat transfer enhancement is further clarified in Fig. 4(b). However, it is noted that the change in heat transfer per unit increase in A decreases with increasing A. This indicates that there is a practical limit to the benefit of this heat transfer enhancement mechanism, whereby the benefit of enhancing heat transfer may be outweighed by the cost of increasing A.

To illustrate the role of oscillation and perturbation frequencies on the flow, Fig. 5(a) shows the variation of forcing frequency for maximum heat transfer $St_{e,\max}$ with oscillation amplitude. The figure suggests that as $A \to 0$, the optimal excitation frequency approaches the frequency of the global

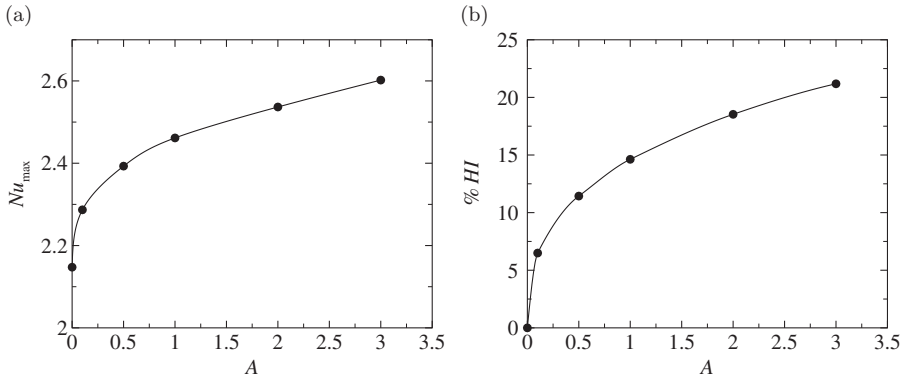

FIG. 4. The variation of (a) peak time-averaged $Nu_{\max}$ over the heated surface, and (b) the percentage increase to the heat transfer plotted against angular velocity amplitude of the cylinder (A) for $Re = 1075$ and $Ha^\star = 151.5$.

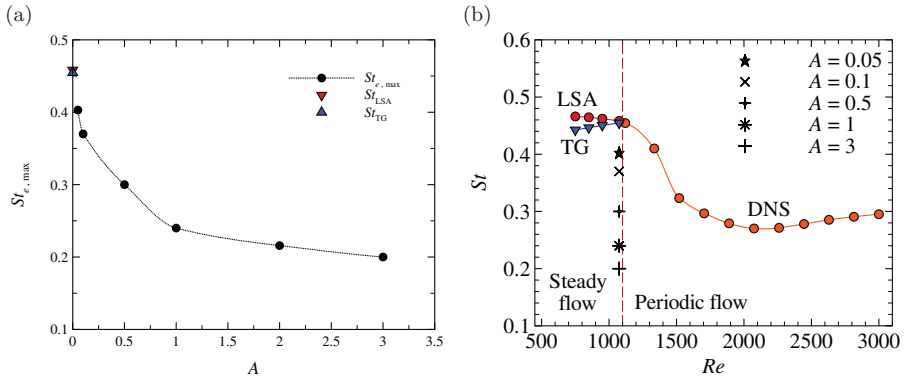

FIG. 5. (a) A plot of oscillation frequency for maximum Nusselt number ($St_{e,\max}$) as a function of angular velocity amplitude of the cylinder. (b) A plot of shedding frequency St against Re showing the natural frequency predicted by linear stability, DNS, and transient growth analyses, as labeled. The data from (a) are included at $Re = 1075$ for comparison.

mode predicted from linear stability analysis. Fig. 5(b) presents the frequency predicted by linear stability analysis (LSA), transient growth (TG) analysis, and direct numerical simulation (DNS) of quasi-two-dimensional flow as a function of Reynolds number. Relatively higher frequencies are observed prior to the onset of vortex shedding. The preferred wake frequency is observed to decrease as the nonlinear regime is entered (either through increasing the Reynolds number, or by imposing a higher-amplitude forcing through oscillation of the cylinder), which also creates large-scale oscillations in the wake, thereby significantly altering the flow from the steady state that formed the basis of the linear stability and transient growth analyses. In addition, it is worth mentioning that the frequencies predicted by LSA and TG are very close, and they intersect near the unsteady transition Reynolds number. This confirms a conclusion of Ref. 17 that the optimal perturbation excites and feeds energy into the global wake mode.

In order to determine the range of driving frequencies where the heat transfer enhancement is considerable, a full width at half maximum (FWHM) analysis is applied. The full width at half maximum is a parameter usually used to describe the width of a peak of a function.[30] It is given by the frequency range at which the function reaches half its maximum value, and its application in the present study is conveyed in Fig. 6. FWHM values obtained at different amplitudes are listed in Table II. These are represented relative to the zero-oscillation baseline, $Nu_s = 2.15$. The results show that FWHM almost doubles as the forcing frequency is increased from 0.1 to 3. Thus, at large amplitudes, the range of forcing frequencies that produce significant heat transfer improvement is higher than for small amplitudes.

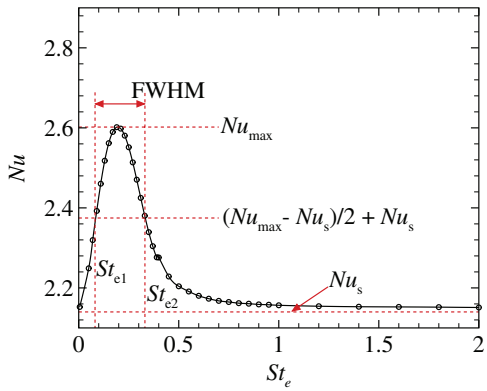

FIG. 6. Nomenclature for calculation of the full width at half maximum (FWHM) of frequencies at $A = 3$ for $Re = 1075$ and $Ha^\star = 151.5$.

TABLE II. Calculated full width at half maximum (FWHM) Strouhal number ranges at different oscillation amplitudes for $Re = 1075$ and $Ha^{\star} = 151.5$.

A	Half max. Nu_{max}	St_{e1}	St_{e2}	FWHM
0.1	2.2171	0.3016	0.4287	0.1271
0.5	2.2702	0.2038	0.3896	0.1858
1.0	2.3044	0.1501	0.3798	0.2298
3.0	2.3747	0.0865	0.3358	0.2493

B. Flow structure and temperature fields

In this section, the effect of a torsional cylinder oscillation on the flow structure and temperature fields are examined. Vorticity contours for different oscillation amplitudes at the frequency of maximum heat transfer augmentation are shown in Fig. 7. For the stationary case, the flow is characterized by a pair of a symmetric counter-rotating vortices on the either side of the wake centerline. The temperature field is time-independent, and the thermal boundary layer is uniform and stable.

At the lowest amplitude of oscillation ($A = 0.1$), a pattern of wake shedding is produced that closely resembles natural vortex shedding in an unperturbed flow above the critical Reynolds number. Note in particular that successive alternately shed vortices align approximately in a single row along the wake centerline. These advecting vortices only weakly interact with the wall boundary layers as they travel downstream (note the visible variation in wall boundary layer thickness between approximately $1d$ and $5d$ downstream of the cylinder). As the cylinder oscillation amplitude is increased to $A = 0.5$, the vortex formation length shortens and the vortices move closer to channel side walls as they convect downstream. In addition, the intensity of vortices increases. The wall shear layers start to entrain inwards to interact with the vortices shed from the cylinder. This effect is further pronounced at $A = 1$, whereas by $A = 3$ the wall shear layers roll up into opposite-sign vortices that pair with wake vortices. These counter-rotating vortex pairs then self-propel inwards from the walls, explaining the increasing heat transfer enhancement with increasing A. It can also be speculated that the reason for the diminishing heat transfer enhancement at larger A may be because this mechanism for inciting advection of the fluid away from the heated wall has a limited capacity for enhancement, and has likely been exhausted by $A = 3$.

In order to better characterize the effect of the vortex patterns on the wall heat transfer, temperature contours are presented in Fig. 7. It is noted that due to the low Prandtl number used in this study (Pr= 0.022), thermal diffusion occurs at a far greater rate (approximately 45 times greater) than

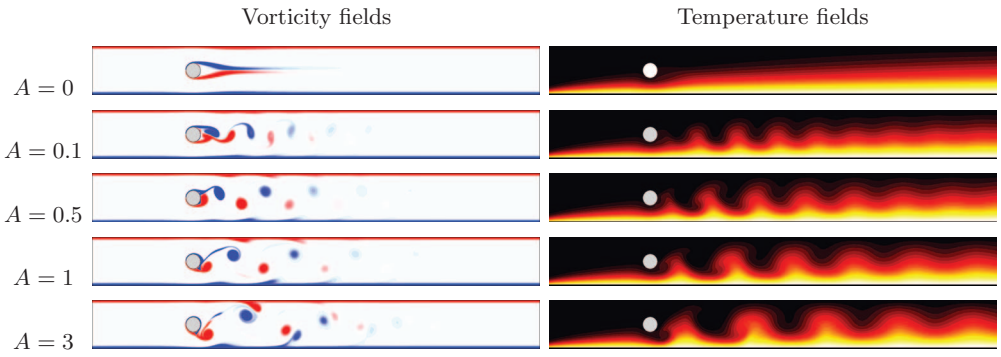

FIG. 7. Contour plots of vorticity (left) and temperature (right) for fixed ($A = 0$) and torsionally oscillating cylinders ($A > 0$) in a channel. Each case is depicted at the frequencies producing maximum heat transfer for $Re = 1075$, $Ha^{\star} = 151.5$, and $\beta = 0.303$, and at the point of the maximum counter-clockwise rotation of the cylinder. Vorticity fields: light and dark gray (red and blue online) contours show positive and negative vorticity, respectively. Temperature fields: dark and light contours show cold and hot fluid, respectively.

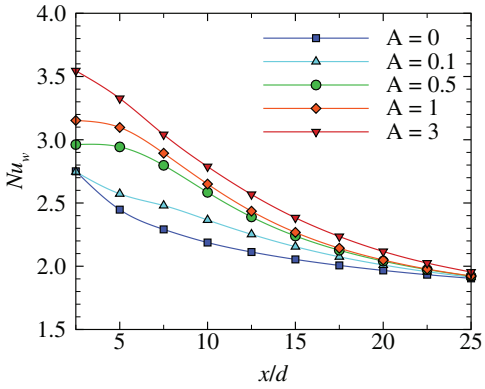

FIG. 8. Local Nusselt number over the heated surface of the side wall and as a function of x/d at different oscillation amplitudes for maximum frequency at $Re = 1075$ and $Ha^{\star} = 151.5$.

viscous diffusion. This explains the diffused "blurry" appearance of the temperature fields. The wavy structures observed in the thermal boundary layers are due to the cross-stream mixing induced by the presence of advecting vortices. The net effect is for low-temperature fluid to be transported toward the hot region of the channel and the high-temperature fluid near the heated wall to be convected away to mix with the low-temperature fluid. This process enhances the mixing between the heated surface and the cold fluid, and as a result the heat transfer is significantly enhanced compared to the stationary cylinder.

Now the local Nusselt number will be considered both as a function of position along the heated duct wall, and variation in A. Fig. 8 presents the distribution of the local Nusselt number Nu_w along the heated surface as a function of stream-wise coordinate x for different oscillation amplitudes. It is found that the effect of oscillation amplitude on the distribution of Nusselt number along the heated wall is significant. The figure shows that as A is increased, there is a progressive increase in Nu_w over a region extending from the cylinder to a distance downstream of the cylinder. It can also be seen that the duct wall region over which the local Nusselt number is increased (compared to $A = 0$) moves upstream. Specifically, as A is increased over 0.1, 0.5, and 1, the point of maximum increase in local Nusselt number advances upstream from approximately $x/d = 10$ to 5. The large oscillation velocity amplitude ($A = 3$) also produces its maximum increase in Nu_w at approximately $x/d = 5$, but it is also notable that unlike the lower oscillation velocity amplitudes, $A = 3$ shows significantly increased local Nusselt number near to the cylinder (i.e., $1 \lesssim x/d \lesssim 2.5$). An explanation for this can be deduced from the vorticity plots shown in Fig. 7, which show that for $A = 3$, the wake vortices are cast to the side walls much nearer to the cylinder than for the smaller amplitudes. As a result, the highest local Nusselt number is observed for the $A = 3$ case. On the other hand, the local Nusselt number measurements upstream of the cylinder are coincident for all velocity amplitudes, where the flow and heat transfer characteristics are very similar. This demonstrates that the heat transfer enhancement benefit is only felt downstream of the cylinder, and this is also reflected in Fig. 7, where no visible differences are apparent in the vorticity and temperature fields upstream of the cylinder.

A notable observation from Fig. 8 is that the enhancement to heat transfer is higher in the near-wake region, where the wake vortices are strongest. Further downstream these vortices decrease in strength rapidly due to Hartmann damping, and the local Nusselt number again approaches that for the steady-state wake case. The predicted enhancement to the time-averaged Nusselt number reported earlier calculated using the entire computational domain length to calculate the spatial average; however, perhaps a more physically based averaging length would be the active wake region. In practice, there would be no reason to use only a single cylinder to enhance heat transfer. Multiple cylinders could be positioned along the duct centreline at regular intervals to regenerate the wake.

Fig. 7 shows that the wake vortices are clearly discernible for only approximately 10 cylinder diameters downstream. Reducing the spatial averaging length to just the $10d$ immediately

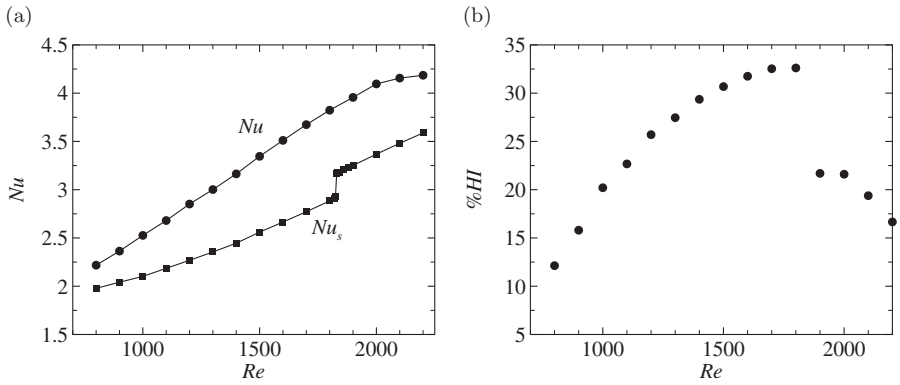

FIG. 9. (a) A plot of Nusselt number over the heated surface against Reynolds number for an oscillating (Nu) and stationary (Nu_s) cylinder. (b) The percentage increase in heat transfer generated by cylinder oscillation over a stationary cylinder as a function of Reynolds number. $A = 3$ and $Ha^\star = 151.5$.

downstream of the cylinder increases the heat transfer enhancement over the base case from 22% to 33% for $A = 3$. For the other rotation speeds, the enhancement is also approximately 50% more.

To further understand the dynamics of this heat transfer enhancement mechanism, the Reynolds number dependence of the flow and heat transfer will now be considered. Reynolds number variation for the cases of a fixed cylinder ($A = 0$) and at ($A = 3$) are considered. Fig. 9 plots the respective Nusselt-number variation for these cases, and the heat transfer increment of the $A = 3$ case over the $A = 0$ case. At $A = 3$, the variation of peak Nusselt number rises approximately linearly with Reynolds number, though beyond $Re \gtrsim 2000$ a reduction in the rate of increase is measured. This high-Reynolds-number plateau is likely indicative of one of two phenomena: either the flow has reached an inertia-dominated regime whereby there is no longer a capacity for further increases in the vortex pairing along the heated boundary drawing heated fluid from the hot duct wall, or a drift between the natural frequency of vortex shedding and the frequency used across these Reynolds numbers is leading to a slightly sub-optimal Nusselt number. The latter phenomenon is consistent with the deviation from the peak Nusselt number frequency in the context of the data displayed in Fig. 3. For the case without cylinder rotation, again the Nu–Re data are linear at lower Reynolds numbers (here, up to $Re \approx 1800$), though both the values and gradient are lower than the $A = 3$ data. Interestingly, there is no perceptible change in the Nusselt number data as Reynolds number increases through the transition to unsteady flow (see also the contour plots in Fig. 10). This reflects the initially limited and gradually increasing flow disturbances near the heated wall as the unsteady vortex shedding develops with increasing Reynolds number. A sharp increase in Nusselt number occurs at $Re \approx 1830$, beyond which the Nusselt number returns to a steady increase with Reynolds number. This jump will be discussed shortly in the context of Fig. 10.

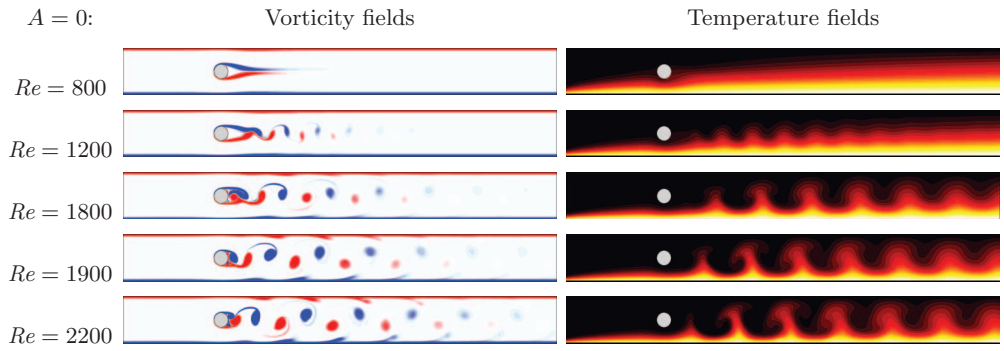

FIG. 10. Vorticity and temperature plots for fixed ($A = 0$) cylinder in a channel at Reynolds numbers as indicated, $Ha^\star = 151.5$ and $\beta = 0.303$. Contours and orientation are as per Fig. 7.

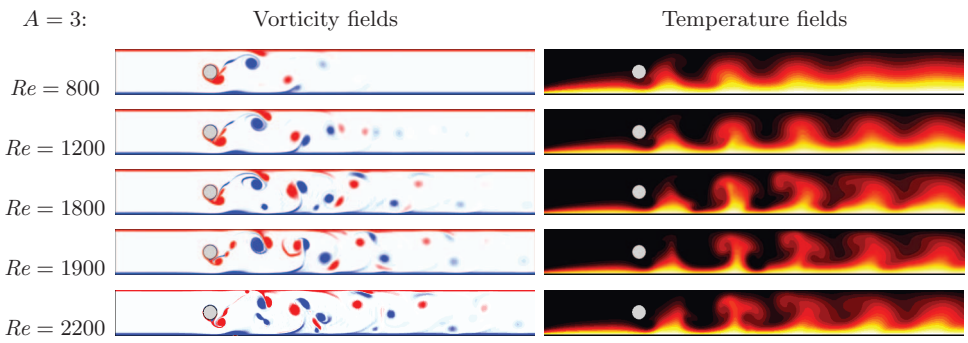

FIG. 11. Vorticity and temperature plots for cylinders rotating with $A = 3$ in a channel at Reynolds numbers as indicated, $Ha^{\star} = 151.5$ and $\beta = 0.303$. Contours, orientation, and phase of cylinder oscillation are as per Fig. 7.

The implications of these Nusselt-number/Reynolds-number trends on the increment of heat transfer invoked by cylinder rotation with $A = 3$ is revealed in Fig. 9(b). The heat transfer increment rises sharply from approximately 12% at $Re = 800$ to approximately 26% at $Re = 1200$, before gradually cresting to a peak of above 32% at $Re \approx 1800$. However, beyond this Reynolds number a sharp drop in $\%HI$ to approximately 20% occurs, corresponding to the increase in Nu_s at these Reynolds numbers in Fig. 9(a).

Contour plots of the vorticity and temperature fields at several Reynolds numbers for the $A = 0$ case are plotted in Fig. 10. These show that the flow is initially steady-state ($Re = 800$), and from $Re = 1200$ and upwards the flow is unsteady, with progressively increasing wake vortex strength with increasing Reynolds number. This is complemented by a progressive increase in the degree of cross-stream mixing of the temperature fields downstream of the cylinder. Comparing with the Nu_s jump at $Re \approx 1830$, this figure demonstrates that this jump is associated with a topological change in the near-wake structure; at $Re = 1800$ the formation length extends approximately $2d$ downstream of the cylinder (and at lower Reynolds numbers longer formation lengths are observed). However, at higher Reynolds numbers, the formation length is very short, with wake vortices developing and shedding from within $1d$ of the rear of the cylinder. Across the Reynolds number range considered here, the continuously increasing Nusselt number for the $A = 0$ case is reflected by a monotonic increase in the evidence of heated wall vorticity (and hot fluid) entrainment into the interior of the channel.

Contour plots of the $A = 3$ cases are plotted in Fig. 11. These frames are consistently displayed at the point of maximum counter-clockwise rotation of the cylinder. At this phase, a positive vortex is developing behind the bottom of the cylinder, and in each frame approximately $3d$ downstream of the cylinder, a negative-signed vortex has paired with a counter-rotating eddy of vorticity drawn from the top wall. From this instant in time, the orientation of this vortex pair will see it convect downwards and to the right, thus carrying fluid from the Shercliff layer into the wake. As the Reynolds number increases, the decay of vortices downstream becomes slower. Particularly evident in the $Re = 1800$ frame and higher, vortex pairs that develop aft of the cylinder at the channel side walls survive long enough to traverse the entire width of the channel, thus demonstrating more effective fluid mixing at higher Reynolds number. This is reflected in the temperature field plots, where again the cross-channel mixing of hot and cold fluid increases with Reynolds number. Notably though, the differences between frames are less pronounced between the $Re = 1900$ and 2200 frames, consistent with the observed high-Reynolds-number plateau in the Nusselt number data for $A = 3$ in Fig. 9(a). Finally, when comparing the same Reynolds numbers between Figs. 10 and 11, consistently the addition of cylinder rotation is seen to enhance the cross-stream mixing, the casting of wake vortices to the side-walls, and the subsequent development of self-propelling counter-rotating vortex pairs. An extension of this observation is that the distance between the cylinder and the hot channel wall is an important feature of this mechanism: channels with smaller blockage ratios may indeed require the cylinder to be offset from the channel centerline nearer to the hot channel wall, though further investigation of this point is beyond the scope of the present paper.

In this paper, a mechanical perturbation of the flow has been explored, but by no means is a mechanical solution the only possibility in MHD duct flows such as these. Numerous studies[3,22,31,32] have perturbed MHD flows using electromagnetic mechanisms by a way of imparting fluctuating currents on the duct flow. An interesting avenue for future exploration would be to combine a fixed turbulence promoter (such as the cylindrical obstacle in the present study) with an electromagnetic perturbation mechanism tuned to the optimal disturbance frequencies[17] to provoke the vortex shedding and enhancement of heat transfer without introducing the complexities of a mechanical oscillation mechanism.

C. Power requirements

Consideration is now given to the mechanical power required to oscillate the cylinder about its axis. The moment of inertia of the cylinder, friction in bearings, and other mechanical losses are not considered. Only the power required to overcome the moment exerted by the flow on the cylinder is considered. Mathematically, this can be determined from the dot product of the moment exerted by the fluid on the cylinder and its angular velocity vector as

$$P(t) = -\mathbf{M}(t) \cdot \dot{\boldsymbol{\theta}}_{\mathrm{cyl}}(t), \tag{17}$$

where the negative sign appearing in Eq. (17) indicates that the power is added to the system to drive the cylinder. Here, both $\mathbf{M}$ and $\dot{\boldsymbol{\theta}}_{\mathrm{cyl}}$ are defined as counterclockwise positive. The time-averaged power is obtained by integrating the instantaneous power over a time interval using

$$P_{\mathrm{avg}} = \frac{-1}{t} \int_0^t \mathbf{M} \cdot \dot{\boldsymbol{\theta}}_{\mathrm{cyl}} \, \mathrm{d}t. \tag{18}$$

The time variation of the moment and mechanical power required to drive the cylinder for different velocity amplitudes at peak heat transfer frequencies are presented in Fig. 12 for different velocity amplitudes at the maximum frequency. From Fig. 12(a), a significant phase-shift in the moment is observed as A increases. Therefore, it is expected that the power required to oscillate the cylinder grows significantly as A increases. The time variation of power in Fig. 12(b) indicates that of the cases inspected here, the minimal power requirement occurs for $A = 0.5$. This is likely related to the fact that the forcing frequency at small amplitude approaches the frequency of the global mode (see Fig. 5), resulting in the flow resembling that of stationary confined cylinder above the shedding transition.

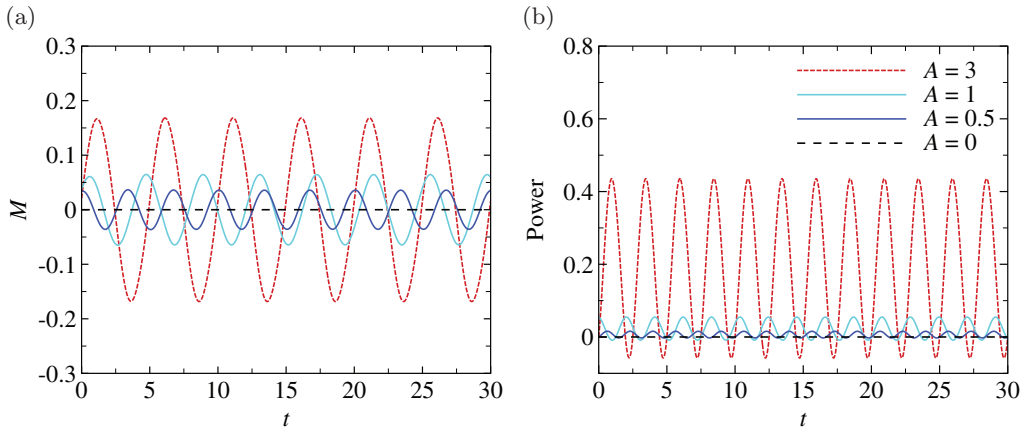

FIG. 12. Time variation of (a) the moment and (b) the power required to drive the cylinder for $A = 0.5$, 1, and 3 at the optimal frequency.

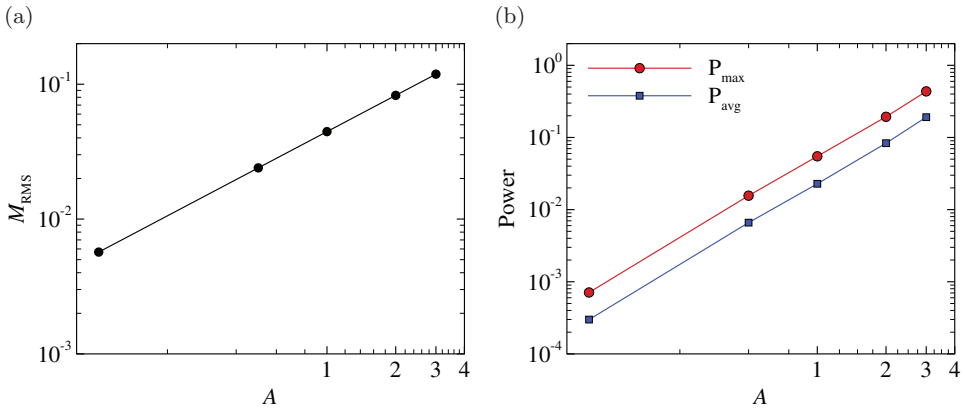

FIG. 13. (a) The root mean square of the moment M_{RMS}, (b) time-averaged and maximum power required to drive the cylinder, both plotted on logarithmic scales against A.

To quantify the magnitude of oscillations in the moment time history, which are not necessarily perfectly sinusoidal, a root mean square (RMS) measure of the moment is employed, defined as

$$M_{\mathrm{RMS}} = \sqrt{\frac{1}{t}\int_0^t [M(t)]^2 \, \mathrm{d}t}. \tag{19}$$

It is found that M_{RMS} increases almost 321%, 682%, and 1986% as A changes from 0.1 to 0.5, 1, and 3, respectively. The variation of M_{RMS} with A is shown in Fig. 13(a), which follows a power law relationship that is given by

$$M_{\mathrm{RMS}} \approx 0.045 \, A^{0.89}. \tag{20}$$

The variation in the time-averaged and maximum power are provided in Fig. 13. The linear profiles on the log-log scale used in the figure reveals that the average and maximum powers increase significantly with increasing A, and they scale with approximately the 1.9^{th} power of A. The relations between the power and amplitude are found to be

$$P_{\mathrm{max}} \approx 0.055 \, A^{1.88}, \tag{21}$$

$$P_{\mathrm{avg}} \approx 0.023 \, A^{1.89}. \tag{22}$$

Interestingly, here $P \propto A^{1.9}$, while Eq. (20) gives $M \propto A^{0.9}$. These combine to give $P \propto M \times A$, which follows from Eq. (15), as A is a measure of the angular velocity appearing in Eq. (17).

To quantify the power required to torsionally oscillate the cylinder against the flow, a comparison is made to the power required to pump the fluid through the channel. The time-averaged pumping power is calculated using the pressure drop across the channel for the fixed and torsionally oscillated cylinder. The pumping power $P_{\Delta p}$, listed in Table III, increases with increasing velocity amplitude of the cylinder. Not surprisingly, the larger velocity amplitude ($A = 3$) results in only 3.5% increase

TABLE III. Pumping power required to drive fluid in the channel ($P_{\Delta P}$) and the time-averaged power required to oscillate the cylinder, for $Re = 1075$ and $Ha^{\star} = 151.5$.

A	$P_{\Delta p}$	P_{avg}
0.0	1.93	0.0
0.1	1.94	2.99×10^{-4}
0.5	1.96	6.60×10^{-3}
1.0	1.97	2.28×10^{-2}
3.0	2.01	1.91×10^{-1}

in the pumping power compared to that for a stationary cylinder, and the power required to oscillate the cylinder is about two order of magnitudes lower than for the pumping power. Using the data given in Table III, the increases in power compared with the stationary case are approximately 3% and 13% for $A = 1$ and 3, respectively. For $A \leq 0.5$, the increase is almost negligible.

V. CONCLUSIONS

In this study, a mechanism for heat transfer enhancement in the steady flow regime due to damping at high Hartmann number involving the rotational oscillation of a cylinder placed in a duct is proposed and investigated over a wide range of oscillation amplitudes and forcing frequencies. The motivation for exploring this mechanism was inspired by a recent transient growth analysis,[17] which indicated that the optimal disturbances are localized near the cylinder and are characterized by an asymmetrical disturbance with respect to the wake centreline.

It is found that heat transfer is enhanced by increasing one or both of the amplitude of torsional oscillation and the Reynolds number, and carefully tuning the oscillation frequency to optimize the heat transfer.

The results show that there is a considerable increase in heat transfer from the heated channel wall due to rotational oscillation of the cylinder, with maximum enhancement of almost 22% observed for the highest amplitude case examined over steady flow, increasing to more than 30% in a zone extending $10d$ downstream of the cylinder. The range of St_e for effective enhancement was widened, and the frequency at which the peak Nusselt number occurred was shifted slightly to the lower frequency, as A was increased. It was found that as the amplitude was reduced, the optimal forcing frequency approached the frequency of the global mode. A FWHM analysis showed that for the largest amplitude case the range of forcing frequencies that produced higher augmentation in heat transfer was approximately 100% larger than for the smallest amplitude case.

The wake vorticity and temperature contours were found to be closely related. As the amplitude was increased, the formation of strong discrete wake vortices induced the wall boundary layers to be drawn away from the walls enhancing heat transfer. The effect of oscillation amplitude on the distribution of local Nusselt number Nu_w along the heated wall was significant. For small A, the distribution was found to be similar to that for a fixed cylinder (i.e., $A = 0$). However, for large A, significant enhancement occurred in the cylinder near the wake before dropping away further downstream.

Calculations of the power required to oscillate the cylinder indicated that the demands of time-averaged and maximum power significantly increased as the velocity amplitude of oscillation increased from $A = 0.1$ to 3, scaling with approximately the 1.9^{th} power of A. For the largest amplitude, a modest increase in the pumping power of 3.5% was predicted compared to that for the stationary cylinder. The power required to oscillate the cylinder was about two order of magnitudes lower than that for the pumping power.

Given that the improvement in heat transfer enhancement asymptotes with increasing A, and that the power requirement increases more steeply with increasing A, it is apparent that there will certainly be a practical limit to the available benefit obtained by implementing a mechanism such as that proposed here.

ACKNOWLEDGMENTS

This work is supported by the Australian Research Council through Discovery (Grant No. DP120100153), a high-performance computing time allocation through the National Computational Infrastructure (NCI) Merit Allocation Scheme, and a Monash University Faculty of Engineering Seed Grant. W.K.H. was supported by a scholarship from the Ministry of Higher Education and Scientific Research through the Federal Government of Iraq.

[1] S. Münevver, "Magnetohydrodynamic flow in a rectangular duct," Int. J. Numer. Methods Fluids **7**, 697–718 (1987).
[2] J. Sommeria and R. Moreau, "Why, how, and when, MHD turbulence becomes two-dimensional," J. Fluid Mech. **118**, 507–518 (1982).

[3] J. Moreau and R. Sommeria, "Electrically driven vortices in a strong magnetic field," J. Fluid Mech. **189**, 553–569 (1988).
[4] L. G. Kit, S. V. Turuntaev, and A. B. Tsinober, "Investigation with a conduction anemometer of the effect of a magnetic field on disturbances in the wake of a cylinder," Magn. Gidrodin. **6**(3), 35–40 (1970). English translation: Magnetohydrodynamics 6(3), 331–335 (1970).
[5] Y. B. Kolesnikov and A. B. Tsinober, "Two-dimensional turbulent flow behind a circular cylinder," Magn. Gidrodin. **8**(3), 23–31 (1972). English translation: Magnetohydrodynamics 8(3), 300–307, 1972.
[6] D. D. Papailiou, "Magneto-fluid-mechanic turbulent vortex streets," Prog. Astronaut. Aeronaut. **100**, 152–173 (1985).
[7] M. Frank, L. Barleon, and U. Müller, "Visual analysis of two-dimensional magnetohydrodynamics," Phys. Fluids **13**, 2287–2295 (2001).
[8] B. Muck, C. Gunther, U. Müller, and L. Bühler, "Three-dimensional MHD flows in rectangular ducts with internal obstacles," J. Fluid Mech. **418**, 265–295 (2000).
[9] V. Dousset and A. Pothérat, "Numerical simulations of a cylinder wake under a strong axial magnetic field," Phys. Fluids **20**, 017104 (2008).
[10] L. Barleon, U. Burr, R. Stieglitz, and M. Frank, "Heat transfer of a MHD flow in a rectangular duct," in *Transfer Phenomena in Magnetohydrodynamic and Electroconducting Flows: Selected Papers of the PAMIR Conference held in Aussois, France, 22-26 September 1997*, Fluid Mechanics and its Applications Vol. 51, edited by A. Alemany, P. Marty, and J. P. Thibault (Kluwer Academic, Aussois, France, 1997), pp. 305–309.
[11] W. K. Hussam, M. C. Thompson, and G. J. Sheard, "Dynamics and heat transfer in a quasi-two-dimensional MHD flow past a circular cylinder in a duct at high Hartmann number," Int. J. Heat Mass Transfer **54**, 1091–1100 (2011).
[12] L. Barleon, U. Burr, K.-J. MacK, and R. Stieglitz, "Heat transfer in liquid metal cooled fusion blankets," Fusion Eng. Des. **51–52**, 723–733 (2000).
[13] U. Burr, L. Barleon, U. Müller, and A. Tsinober, "Turbulent transport of momentum and heat in magnetohydrodynamic rectangular duct flow with strong sidewall jets," J. Fluid Mech. **406**, 247–279 (2000).
[14] S.-J. Yang, "Numerical study of heat transfer enhancement in a channel flow using an oscillating vortex generator," Heat and Mass Transfer **39**(3), 257–265 (2003).
[15] W.-S. Fu and B.-H. Tong, "Numerical investigation of heat transfer characteristics of the heated blocks in the channel with a transversely oscillating cylinder," Int. J. Heat Mass Transfer **47**, 341–351 (2004).
[16] B. Celik, M. Raisee, and A. Beskok, "Heat transfer enhancement in a slot channel via a transversely oscillating adiabatic circular cylinder," Int. J. Heat Mass Transfer **53**, 626–634 (2010).
[17] W. K. Hussam, M. C. Thompson, and G. J. Sheard, "Optimal transient disturbances behind a circular cylinder in a quasi-two-dimensional magnetohydrodynamic duct flow," Phys. Fluids **24**, 024150 (2012).
[18] U. Müller and L. Bühler, *Magnetofluiddynamics in Channels and Containers* (Springer, New York, 2001).
[19] G. J. Sheard and M. P. King, "The influence of height ratio on Rayleigh-number scaling and stability of horizontal convection," Appl. Math. Model **35**, 1647–1655 (2011).
[20] M. A. Hossain, "Viscous and Joule heating effects on MHD-free convection flow with variable plate temperature," Int. J. Heat Mass Transfer **35**, 3485–3487 (1992).
[21] H. S. Yoon, H. H. Chun, M. Y. Ha, and H. G. Lee, "A numerical study on the fluid flow and heat transfer around a circular cylinder in an aligned magnetic field," Int. J. Heat Mass Transfer **47**, 4075–4087 (2004).
[22] Y. B. Kolesnikov and O. V. Andreev, "Heat-transfer intensification promoted by vortical structures in closed channel under magnetic field," Exp. Therm. Fluid Sci. **15**, 82–90 (1997).
[23] N. B. Morley, S. Smolentsev, L. Barleon, I. R. Kirillov, and M. Takahashi, "Liquid magnetohydrodynamics—Recent progress and future directions for fusion," Fusion Eng. Des. **51-52**, 701–713 (2000).
[24] Y. T. Chew, M. Cheng, and S. C. Luo, "A numerical study of flow past a rotating circular cylinder using a hybrid vortex scheme," J. Fluid Mech. **299**, 35–71 (1995).
[25] G. J. Sheard, K. Hourigan, and M. C. Thompson, "Computations of the drag coefficients for low-Reynolds-number flow past rings," J. Fluid Mech. **526**, 257–275 (2005).
[26] G. E. Karniadakis, M. Israeli, and S. A. Orszag, "High-order splitting methods for the incompressible Navier–Stokes equations," J. Comput. Phys. **97**, 414–443 (1991).
[27] A. Neild, T. W. Ng, G. J. Sheard, M. Powers, and S. Oberti, "Swirl mixing at microfluidic junctions due to low frequency side channel fluidic perturbations," Sens. Actuators B **150**, 811–818 (2010).
[28] G. J. Sheard, "Wake stability features behind a square cylinder: Focus on small incidence angles," J. Fluids Struct. **27**, 734–742 (2011).
[29] F. M. Mahfouz and H. M. Badr, "Forced convection from a rotationally oscillating cylinder placed in a uniform stream," Int. J. Heat Mass Transfer **43**, 3093–3104 (2000).
[30] S. W. Smith, *Digital Signal Processing: A Practical Guide for Engineers and Scientists* (Newnes, Oxford, 2003).
[31] L. Bühler, "Instabilities in quasi-two-dimensional magnetohydrodynamic flows," J. Fluid Mech. **326**, 125–150 (1996).
[32] H. Huang and B. Li, "Heat transfer enhancement of MHD flow by conducting strips on the insulating wall," J. Heat Transfer **133**, 021902 (2011).